Supplementary Information

Multicomponent Approach for Stable Methylammonium-Free Tin-Lead Perovskite Solar Cells

Silver-Hamill Turren-Cruz,[1,2,7]* Jorge Pascual,[2,4] Shuaifeng Hu,[2,3] Jesus Sanchez-Diaz,[1] Sergio Galve-Lahoz,[1,4] Wentao Liu,[2] Wolfram Hempel,[5] Vladimir S. Chirvony,[6] Juan P. Martinez-Pastor,[6] Pablo P. Boix,[6] Atsushi Wakamiya,[2]* and Iván Mora-Seró[1]*

[1]Institute of Advanced Materials (INAM), University Jaume I, Av. Vicent Sos Baynat, s/n, 12071, Castellón de la Plana, Spain

[2]Institute for Chemical Research, Kyoto University, Gokasho Uji Kyoto 611-0011, Japan

[3]Clarendon Laboratory, Department of Physics, University of Oxford, Oxford OX1 3PU, U.K.

[4]Polymat, University of the Basque Country UPV/EHU, 20018 Donostia-San Sebastian, Spain

[5]Zentrum für Sonnenenergie- und Wasserstoff-Forschung Baden-Württemberg (ZSW), 70563 Stuttgart, Germany

[6]Instituto de Ciencia de los Materiales (ICMUV), Universidad de Valencia, C/Catedrático José Beltrán 2, E-46980 Paterna, Spain

[7]Department of Physical Chemistry, Polish Academy of Sciences, Warsaw 01-224, Poland

*Corresponding authors: silver.turren@gmail.com, wakamiya@scl.kyoto-u.ac.jp, sero@uji.es

Materials

Unless otherwise stated, all materials were used as received without further purification. Methylammonium iodide (MAI, >99.0%), formamidinium iodide (FAI, >98.0%), bathocuproine (BCP), lead(II) iodide (PbI_2, 99.99%, trace metals basis), and cesium iodide (CsI, >99%) were purchased from Tokyo Chemical Industry Co., Ltd. (TCI). Dipropylammonium iodide (DipI) and 4-fluorophenethylammonium chloride (4FPEACl, >99%), were purchased from Greatcell Solar Materials. Tin(II) fluoride (SnF_2, 99%), tin(II) iodide (SnI_2, beads, 99.99%, trace metals basis), sodium borohydride ($NaBH_4$, ≥98.0%) and rubidium iodide (RbI, 99.9% trace metals basis) were purchased from Sigma-Aldrich Co., Ltd. (Sigma-Aldrich). Poly(3,4-ethylenedioxythiophene)-poly(styrenesulfonate) (PEDOT:PSS) aqueous solution (Clevious PVP AI 4083) was purchased from Heraeus Co., Ltd. Fullerene C_{60} (sublimed, 99.99%) was purchased from ATR Company. Dehydrated dimethyl sulfoxide (DMSO, super dehydrated) and isopropanol (IPA, super dehydrated) were purchased from FUJIFILM Wako Pure Chemical Co., Ltd. Dimethylformamide (DMF), toluene and chlorobenzene were purchased from Kanto Chemical. Co., Inc. All of these solvents were degassed by Ar gas bubbling for 1 h and further dried with molecular sieves (3 Å) in an Ar-filled glove box (H_2O, O_2 <0.1 ppm) before use.

Device fabrication

Substrate cleaning

Glass/FTO substrates (10 Ωsq^{-1}, AGC Inc.) were etched with zinc powder and HCl (6 M in deionized water), and consecutively cleaned with 15 min ultrasonic bath in water, acetone, detergent solution (Semico Clean 56, Furuuchi chemical), water, and isopropanol, followed by drying with an air gun, and finally plasma treatment.

Hole transport layer deposition

The PEDOT:PSS hole transport layer was fabricated from an aqueous dispersion which was filtered through a 0.45 μm PVDF filter and then spin coated on the FTO substrate using a spin program of 10 s

at 500 rpm followed by 30 s at 4000 rpm. The films were then annealed in air at 140°C for 20 min. After transferring to an Ar-filled glove box (H_2O, O_2 <0.1 ppm), the substrates were degassed at 140°C for 30 min.

Perovskite precursor solution

The perovskite film was prepared in an Ar-filled glove box (H_2O, O_2 <0.1 ppm).

MA-containing perovskites

CsFAMA precursor solution

The $Cs_{0.2}FA_{0.7}MA_{0.1}Sn_{0.5}Pb_{0.5}I_3$ perovskite precursor solution was prepared by mixing CsI (98.5 mg, 0.38 mmol), FAI (228.7 mg, 1.33 mmol), MAI (30.2 mg, 0.19 mmol), SnI_2 (353.9 mg, 0.95 mmol), SnF_2 (14.9 mg, 0.095 mmol) and PbI_2 (438.0 mg, 0.95 mmol) in a solvent mix of 0.25 mL of DMSO and 0.75 mL of DMF, to reach a concentration of 1.9 M, and was stirred overnight at room temperature.

CsFAMA precursor solution with RbI (RbCsFAMA)

The $Rb_{0.01}Cs_{0.2}FA_{0.7}MA_{0.1}Sn_{0.5}Pb_{0.5}I_3$ perovskite precursor solution was prepared by adding RbI (4.0 mg, 0.019 mmol) into CsFAMA precursor solution, prepared in a solvent mix of 0.25 mL of DMSO and 0.75 mL of DMF to reach a concentration of 1.9 M, and was stirred overnight at room temperature.

MA-free perovskites

CsFA precursor solution

The $Cs_{0.2}FA_{0.8}Pb_{0.5}Sn_{0.5}I_3$ perovskite precursor solution was prepared by mixing CsI (98.5 mg, 0.38 mmol), FAI (261.4 mg, 1.52 mmol), SnI_2 (353.9 mg, 0.95 mmol), SnF_2 (14.9 mg, 0.095 mmol), and PbI_2 (438.0 mg, 0.95 mmol) in a solvent mix of 0.25 mL of DMSO and 0.75 mL of DMF to reach a concentration of 1.9 M, and was stirred overnight at room temperature.

CsFA precursor solution with RbI (RbCsFA)

The $Rb_{0.01}Cs_{0.2}FA_{0.8}Pb_{0.5}Sn_{0.5}I_3$ perovskite precursor solution was prepared by adding 1 mol% RbI (3.9 mg, 0.019 mmol) into CsFA precursor solution, prepared in a solvent mix of 0.25 mL of DMSO and 0.75 mL DMF to reach a concentration of 1.9 M, and stirred overnight at room temperature.

CsFA precursor solution with NaBH$_4$ (CsFA-Na)

0.4 mol% NaBH$_4$ (0.1 mg, 0.004 mmol) was added into CsFA precursor solution, prepared in a solvent mix of 0.25 mL of DMSO and 0.75 mL of DMF to reach a concentration of 1.9 M, and was stirred overnight at room temperature.

CsFA precursor solution with DipI (CsFA-DipI)

The $Dip_{0.02}(Cs_{0.2}FA_{0.8})_{0.29}(Sn_{0.5}Pb_{0.5})_{0.3}I_{0.91}$ (n=30) precursor solution was prepared by mixing of DipI (29.0 mg, 1.40 mmol), CsI (95.2 mg, 0.38 mmol), FAI (252.7 mg, 1.52 mmol), SnI$_2$ (353.9 mg, 0.95 mmol), SnF$_2$ (14.9 mg, 0.095 mmol), and PbI$_2$ (438.0 mg, 0.95 mmol) in a solvent mix of 0.25 mL of DMSO and 0.75 mL of DMF to reach a concentration of 1.9 M, and was stirred overnight at room temperature.

CsFA precursor solution with all additives (RbCsFA-Multi)

The $Rb_{0.01}(Dip_{0.02}(Cs_{0.2}FA_{0.8})_{0.29}(Sn_{0.5}Pb_{0.5})_{0.3}I_{0.91})_{0.99}+(NaBH_4)_{0.002}$ precursor solution was prepared by mixing RbI (3.9 mg, 0.019 mmol), CsI (95.2 mg, 0.38 mmol), FAI (252.7 mg, 1.52 mmol), DipI (29.0 mg, 1.40 mmol), NaBH$_4$ (0.1 mg, 0.004 mmol), SnI$_2$ (353.9 mg, 0.95 mmol), SnF$_2$ (14.9 mg, 0.095 mmol), and PbI$_2$ (438.0 mg, 0.95 mmol) in a solvent mix of 0.25 mL of DMSO and 0.75 mL of DMF to reach a concentration of 1.9 M, and was stirred overnight at room temperature.

Perovskite layer deposition

The precursor solution was stirred at 45°C for 10 min and filtered through a 0.20 μm PTFE filter before use. 200 μL of the precursor solution at room temperature was applied onto the substrate to spin coat the films. A two-step spin coating program was used. The first step was at 1000 rpm for 10 s with an acceleration of 200 rpm s^{-1}, and the second step was at 4000 rpm for 40 s with an acceleration of 1000 rpm s^{-1}. Room-temperature chlorobenzene (400 μL) was used as the antisolvent. The chlorobenzene

was quickly dripped onto the surface of the spinning substrate over an interval of 1 s during the second spin coating step at 20 s before the end of the procedure. The substrate was then immediately annealed on a hot plate at 100°C for 10 min, followed by another step at 65°C for over 10 min. For the 4FPEACl post-treated devices, 3.0 mg 4FPEACl was dissolved in a solvent mix of 1.0 mL of IPA and 1.0 mL of toluene. The mixed solvent solution was stirred at 45°C for 30 min and then filtered through a 0.20-μm PTFE filter before spin coating. 120 μL of the 4FPEACl solution was applied dynamically to the annealed and cooled perovskite films and spin-coated at 4000 rpm for 20 s with an acceleration of 1333 rpm s^{-1} without annealing.

Electron transport layer (ETL) deposition

The perovskite-coated samples were moved under Ar to a vacuum deposition chamber, where 20 nm of C_{60} (deposition rate 0.01 nm s^{-1}) and 8 nm of BCP (deposition rate 0.01 nm s^{-1}) were deposited by thermal evaporation. The top electrode was prepared by depositing 100 nm of silver (Ag) through a shadow mask. The deposition rate for Ag was firstly set as 0.005 nm s^{-1} to reach 5 nm, then raised to 0.01 nm s^{-1} to reach 20 nm, and finally raised to 0.08 nm s^{-1} to reach the target thickness.

Characterization

SEM analysis

Scanning electron microscopy (SEM) was performed with a Hitachi S8010 ultra-high resolution scanning electron microscope (Hitachi High-Tech Corporation).

UV-Vis

UV–vis absorption measurement was performed with a Shimadzu UV-3600 plus spectrometer (Shimadzu Co., Ltd.).

Steady-state Photoluminescence (PL) and Time-Resolved PL (TRPL)

The PL and TRPL characterization of the different fabricated samples was carried out at room temperature and vacuum conditions, in order to avoid any oxidation effect during the measurements and hence having identical conditions for all samples (that were conveniently packed inside the glove box where they were prepared). The characterization was performed in a 90° excitation-detection backscattering configuration using a high-resolution Edinburgh FLS1000 system using an excitation wavelength of 465 nm produced by a Xe lamp for PL or a supercontinuum pulsed laser (FYLA SCT1000) for TRPL, both filtered by the excitation double monochromator. The detection for both PL and TRPL was performed with a cooled near-infrared photomultiplier (Hamamatsu H10330-75). The overall time resolution was in the range of 0.3-0.4 ns, because any deconvolution was applied for extracting the characteristic decay times.

X-ray Diffraction (XRD)

XRD was characterized on a D4 Endeavour diffractometer from Bruker-AXS, with a Bragg-Brentano (/2) geometry and Cu K radiation (0.15406 nm). The data was collected from 10° to 60° with a step scan of 0.05° and a counting duration of 0.5 s/step.

Time-of-flight secondary ion mass spectrometry (ToF-SIMS)

To record SIMS depth profiling and chemical imaging we used the ToF-SIMS 5 from Iontof. A liquid metal ion gun with a Bi beam of 30 keV in energy was used as the analyzing source, in an area of 50 x 50 μm^2. A sputtering source of a metal gun with cesium (Cs-gun) was used as a second source for sputter removal of material of the sample surface running at 1 keV with a sputter crater of 500 x 500 μm^2.

Dynamic light scattering (DLS)

DLS was conducted with an ELSZ-2000 spectrophotometer (Otsuka Electronics Co., Ltd., Japan). The experiment was conducted after around five hours before the sample preparation, as the sample transporting to, and equipment adjustment in, the company. The refractive indices and viscosity of

the solvent were 1.4405 and 1.1005, respectively, based on the DMF and DMSO with the volume ratio of 3 to 1.

Solar Cell Performance Measurement

Photocurrent–voltage (J–V) curves were measured in a N_2-filled glove box (H_2O, O_2 <0.1 ppm) with an OTENTO-SUN-P1G solar simulator (Bunkoukeiki Co., Ltd.). The light intensity of the illumination source was calibrated using a standard silicon photodiode. Each device was measured with a 10 mV voltage step and a 100 ms time step (i.e. scan rate of 0.1 V s^{-1}) using a Keithley 2400 source meter. The device active area was defined by an optimal mask of 0.0985 cm^2 for the regular devices. Steady-state power output (SPO) measurements were performed by holding the device at the voltage of the maximum power point, as determined by the J–V characteristic, and monitoring the current density over the course of 300 s.

External quantum efficiency (EQE)

EQE and internal quantum efficiency (IQE) spectra were measured with a Bunkoukeiki SMO-250III system equipped with a Bunkoukeiki SM-250 diffuse reflection unit (Bunkoukeiki Co., Ltd.). The incident light intensity was calibrated with a standard SiPD S1337-1010BQ silicon photodiode.

Operational Ageing

Maximum power point tracking (MPPT) and long-term stability measurements in room atmospheric conditions were measured under continuous illumination, using a Xenon lamp, by adjusting the sample-light source distance to set an optical power density of 100 mW cm^{-2}, calibrated with a photodiode. The measurements were performed with an AUTOLAB (PGSTAT30) potentiostat; for the long-term stability measurements, an automatic sequence was set to measure the J–V curves every 2h. For the MPPT measurements, a fixed voltage corresponding to V_{MPP} was applied, which was obtained from the J–V curves, and the electrical current I_{MPP} was monitored over time. V_{MPP} are directly extracted from the J-V curves. It is important to highlight that MPP stability measurements where not

performed using a MPP tracker but at fixed voltage, and consequently strictly speaking our experiment could be considered a quasi-MPP experiment.

Electrochemical Impedance Spectroscopy (EIS)

The EIS was measured by using a Potentiostat Autolab PGSTAT30 employing different filters to change light intensity up to 1 sun. For each voltage point (V_{OC}), EIS was measured with an AC 10 mV voltage perturbation from 1 to 100 mHz. Nova software was used to generate data and Z-View software for modeling the equivalent circuit model used to fit the spectra, respectively.

Supplementary Figures
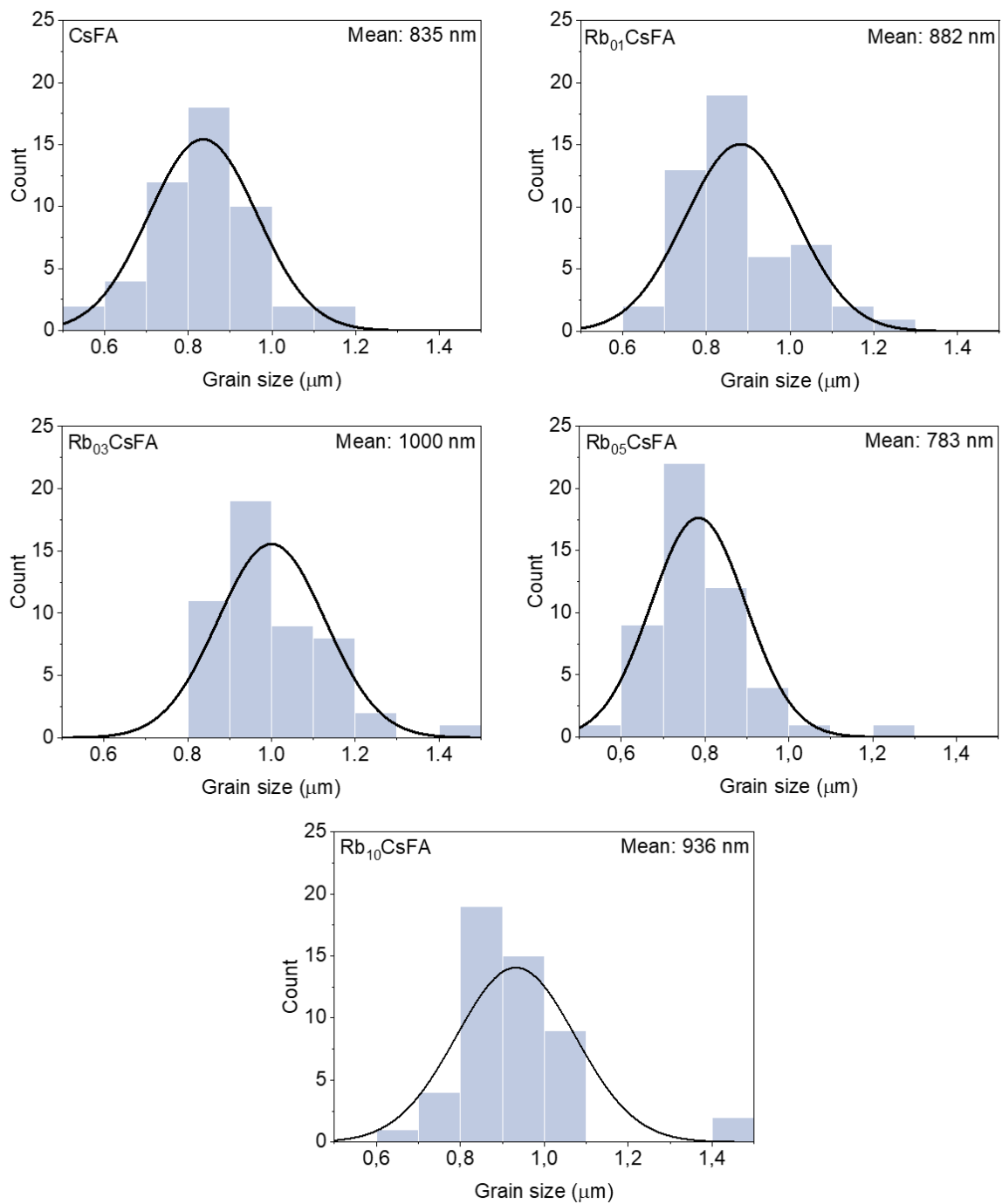
Figure S1. Grain size distribution histograms of CsFA perovskite films with different amounts of RbI (1, 3, 5 and 10 mol%).

$Cs_{20}FA_{80}$	$Rb_{01}(Cs_{20}FA_{80})_{99}$	$Cs_{20}FAMA$	$Rb_{01}Cs_{20}FAMA$
824 nm	1082 nm	882 nm	891 nm
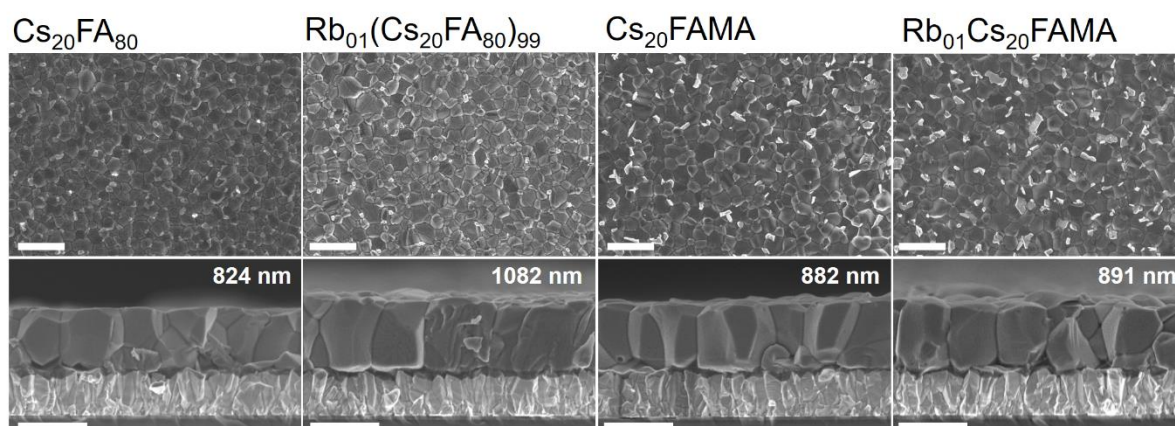
Figure S2. Top and cross section SEM images of perovskite films with CsFA, RbCsFA, CsFAMA and RbCsFAMA compositions at 1.8 M. The scale bars represent 1 μm.
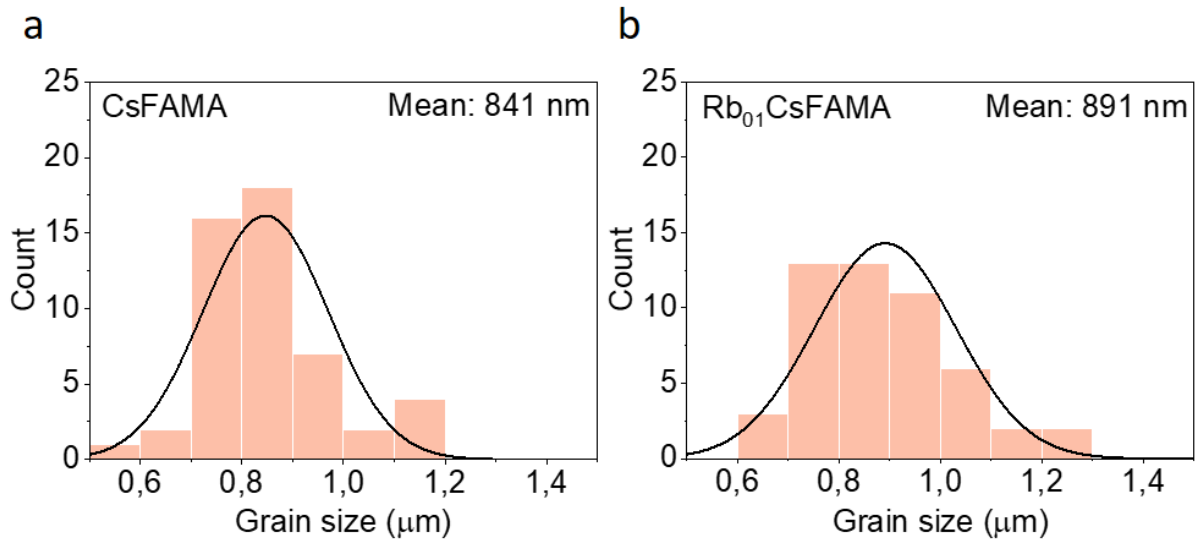
Figure S3. Grain size distribution histograms of a) CsFA perovskite films with MA and b) with MA and Rb.
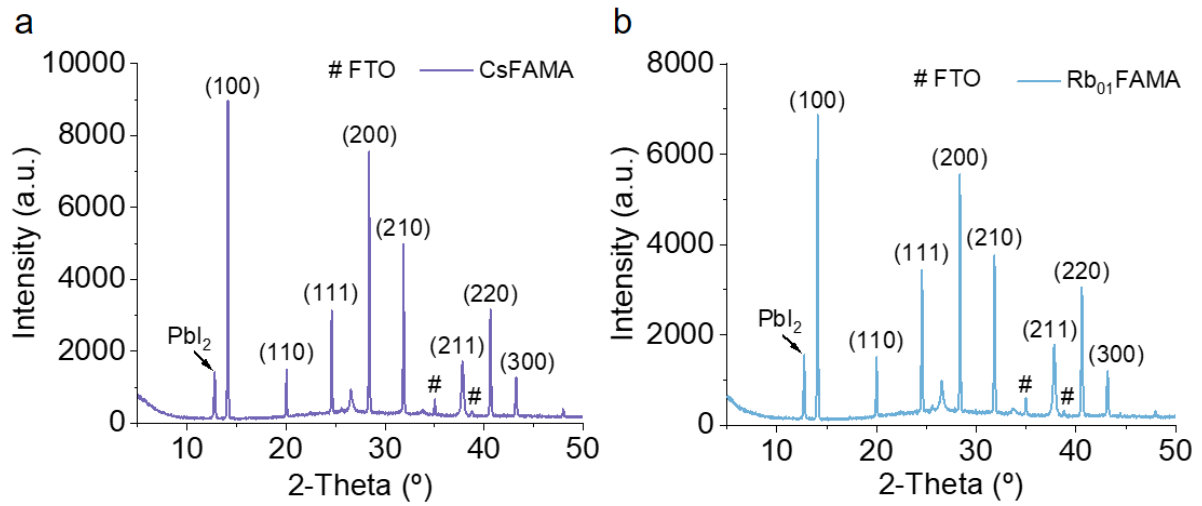
Figure S4. XRD measurements for perovskite films with the different compositions a) CsFA with MA and b) with MA and RbI at 1.8 M. The PbI_2 peaks are indicated with an arrow in the figure and the corresponding perovskite reflections have been assigned.
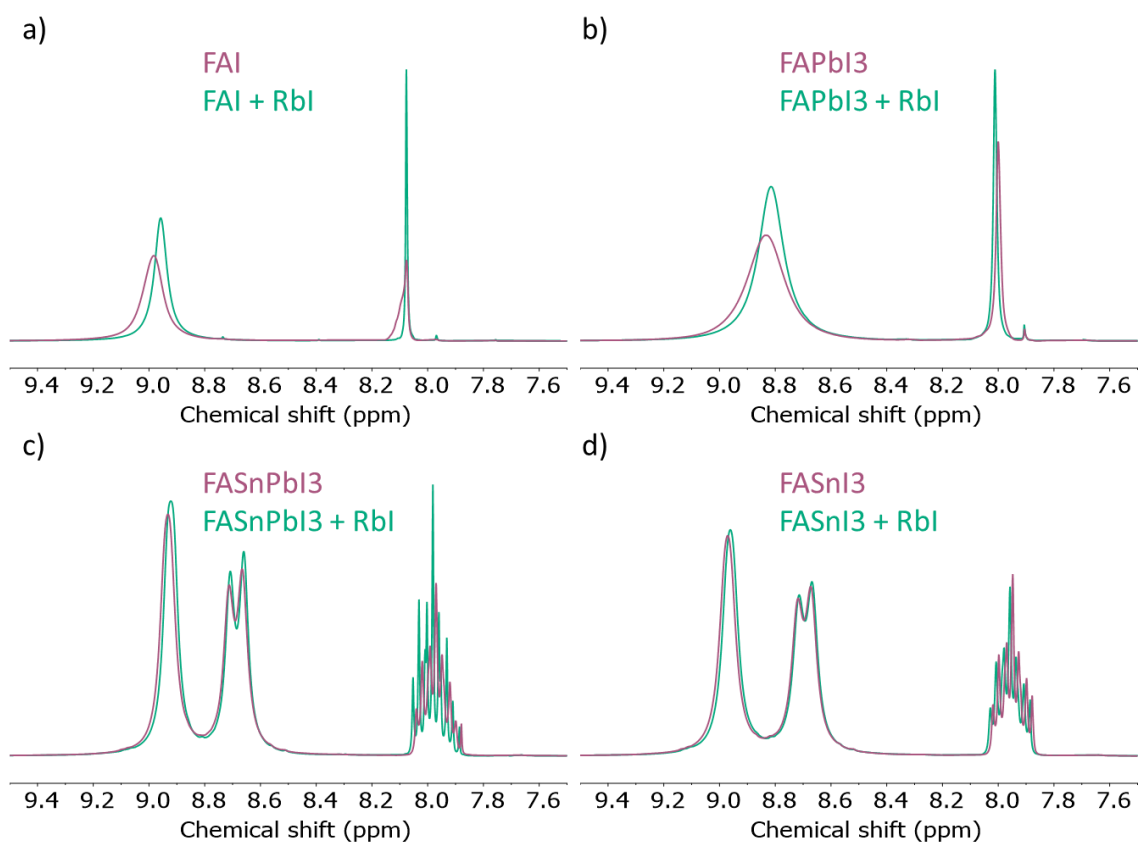
Figure S5. ^{1}H NMR spectra of FA in perovskite precursor solutions with and without RbI addition for a) FAI, b) $FASn_{0.5}Pb_{0.5}I_3$, c) $FAPbI_3$, and d) $FASnI_3$ solutions.

Table S1. Chemical shift of the corresponding FA proton signals and the difference between the control (δ_C) and target (δ_T) samples. δ_{NH2} indicates the central position of the doublet corresponding to the more shielded N-H group.

Sample	δ_{NH2+} (ppm)	$\Delta(\delta_C\text{-}\delta_T)_{NH2+}$ (ppm)	d_{NH2} (ppm)	$\Delta(\delta_C\text{-}\delta_T)_{NH2}$ (ppm)	$\delta_{C\text{-}H}$ (ppm)	$\Delta(\delta_C\text{-}\delta_T)_{C\text{-}H}$ (ppm)
FAI	8,98		-		8,08	
		-0,02		-		0
FAI + RbI	8,96		-		8,08	
FASnPbI₃	8,93		8,69		7,97	
		-0,01		0		0,01
FASnPbI₃ + RbI	8,92		8,69		7,98	
FAPbI₃	8,83		-		8,00	
		-0,02		-		0,01
FAPbI₃ + RbI	8,81		-		8,01	
FASnI₃	8,97		8,70		8,95	
		-0,01		0		0,01
FASnI₃ + RbI	8,96		8,70		8,96	

Figure S6. DLS results for CsFA perovskite precursor solutions with varying concentrations of RbI.

Rb$_{01}$CsFA-Multi
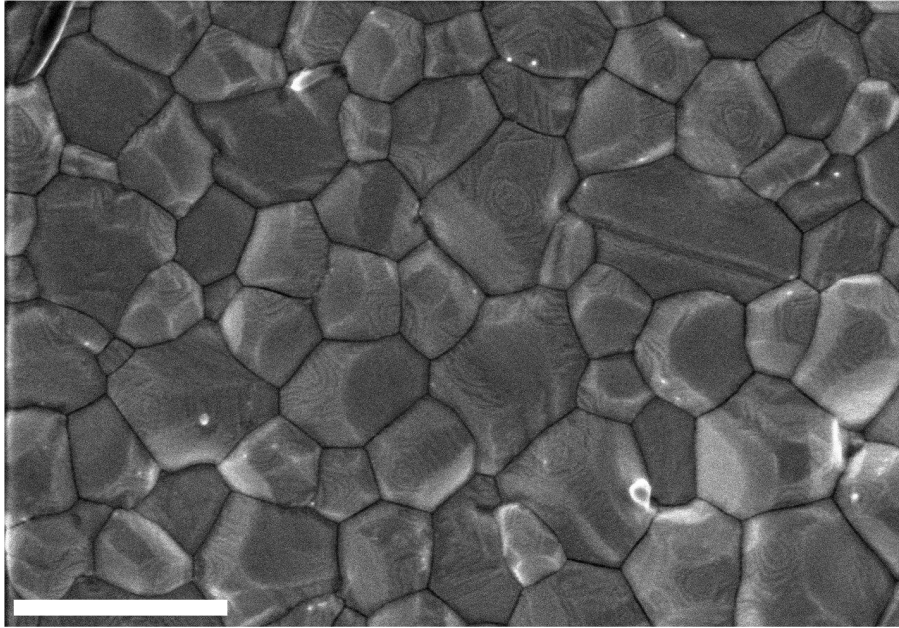
Figure S7. Top SEM image of RbCsFA-Multi (1 mol% RbI) perovskite film. The scale bars represent 1 μm.
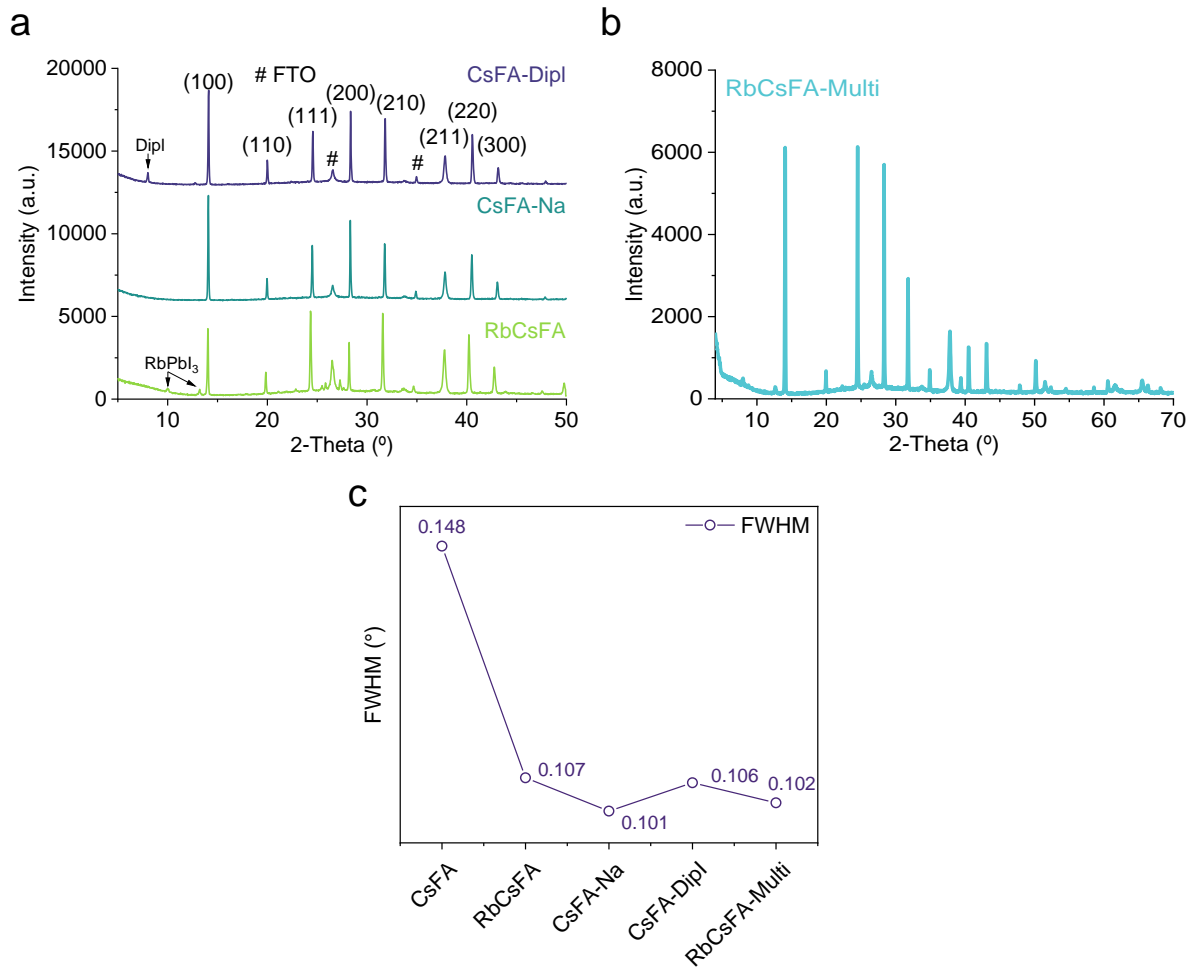
Figure S8. a) XRD measurements for perovskite films with the different additives, b) XRD for MA-free RbCsFA perovskite with all additives and c) peak intensity of the perovskite peak (100) and the full width at half maximum (FWHM) of the main reflection for each sample.
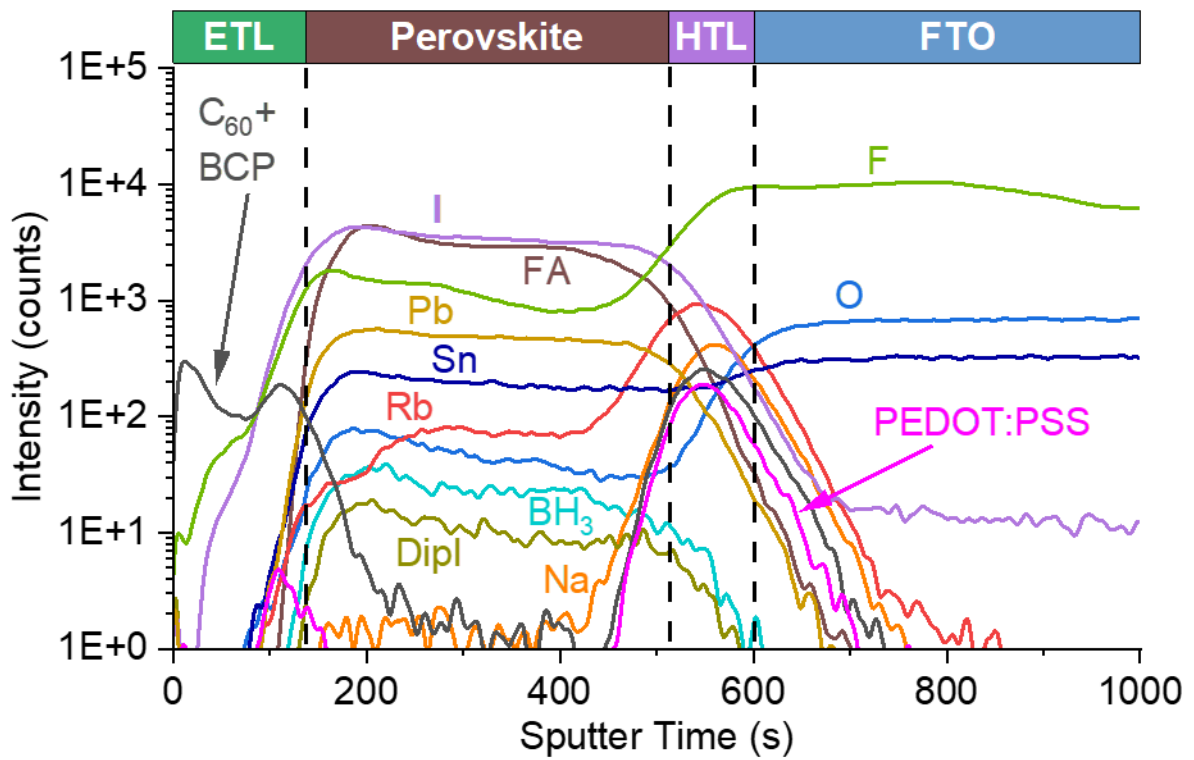
Figure S9. ToF-SIMS measurements of the RbCsFA-Multi perovskite film, showing the depth-dependent compositional distribution. The Cs trace is absent due to using a Cs ion beam during sputtering, which boosted signal intensities.
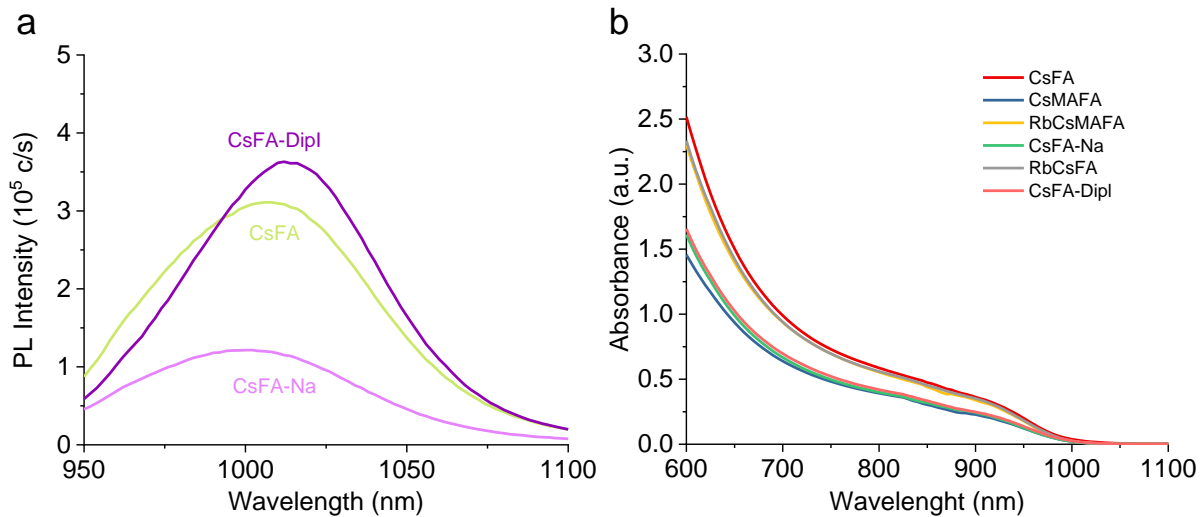
Figure S10. a) PL data for CsFA with $NaBH_4$ and DipI additives and b) UV-vis data for the perovskite with different additives.
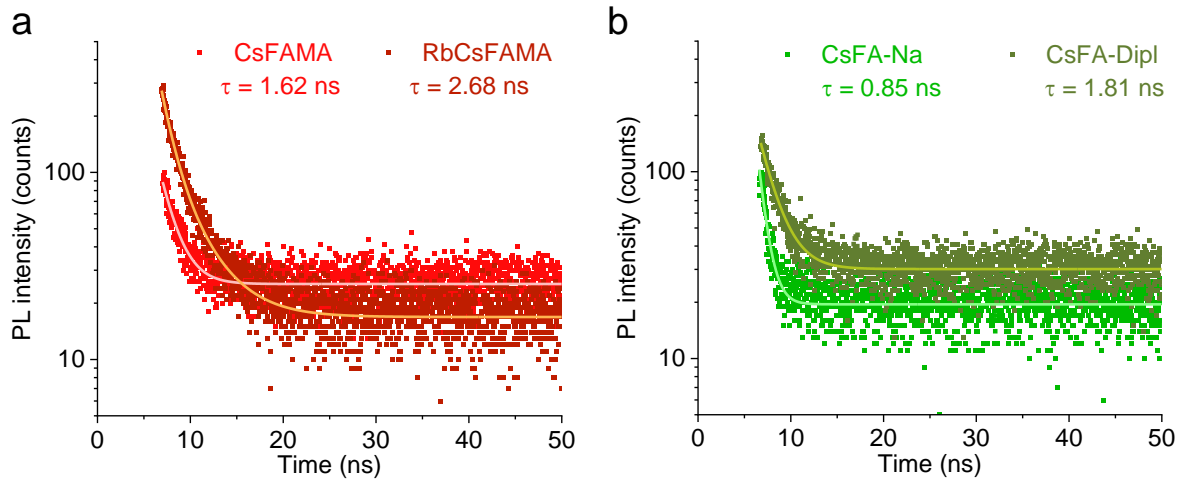
Figure S11. TRPL lifetimes for a) CsFA perovskite films with MA and RbI, and b) CsFA with $NaBH_4$ and Dipl additives.

Table S2. Relative PLQYs and PL lifetimes. Data extracted from the PL decay kinetics in Figures 3d and S11.

Number	Sample type	PLQY (rel)*	PL lifetime** (ns)
1	CsFA	0.22	1.19 (1 exp)
2	CsFAMA	0.10	1.62 (1 exp)
3	RbCsFAMA	0.88	2.68 (2 exp, avg)
4	CsFA-Na	0.085	0.85 (1 exp)
5	RbCsFA	1.0	1.71 (2 exp, avg)
6	CsFA-DipI	0.17	1.81 (1 exp)
7	RbCsFA-Multi	0.85	3.57 (2 exp, avg)

* PLQYs were evaluated on the basis of the PL kinetics in Figures 3d and S11. We suggested that the long-lived background, which is observed for all kinetics, should be the same for all samples independently on its origin. As a measure of PLQY we used the ratio [Integral(S(t)-B)]/B where B is the background value and S(t) is the PL decay kinetics. Then we normalized the ratios to the maximal one obtained for RbCsFA sample.

** Lifetimes are obtained by fitting the PL decay kinetics (Figures 3d and S11) by one- or two-exponential fittings. In the second case, average lifetimes τ_{avg} were calculated by the formula $\tau_{avg} = (\Sigma A_i\tau_i^2/\Sigma A_i\tau_i)$ where A_i is the amplitude of the i-th component (i=1,2).
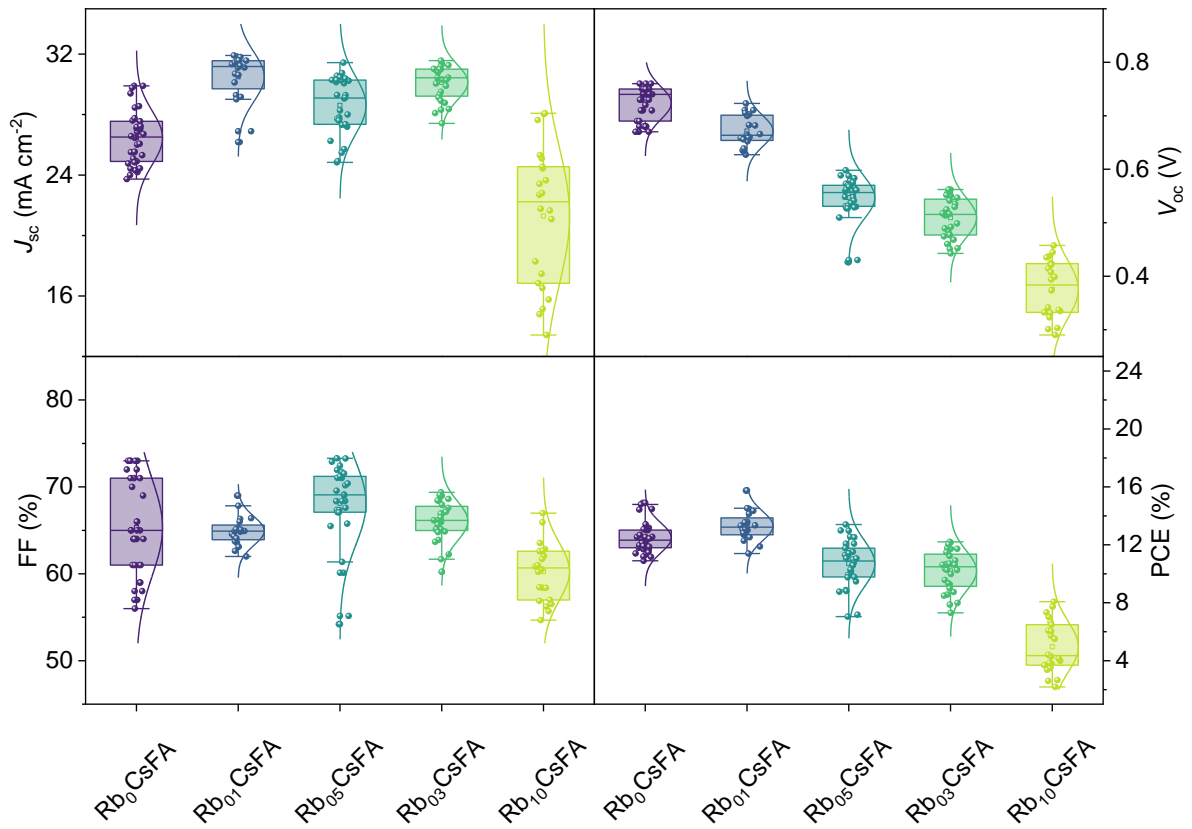
Figure S12. Box plot showing the distribution of the photovoltaic parameters for the solar cells fabricated with CsFA perovskite with different rubidium content at 1.8M.
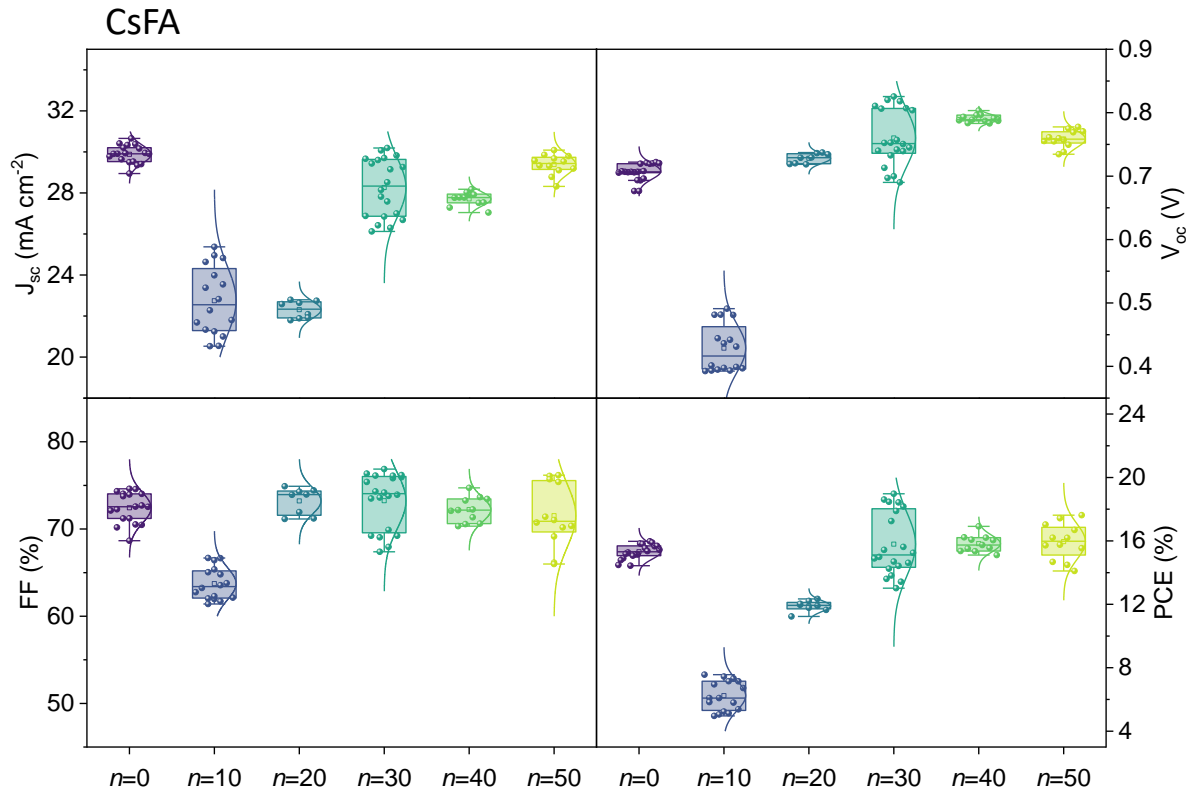
Figure S13. Box plot showing the distribution of the photovoltaic parameters for the solar cells fabricated with CsFA perovskite with different *n* values of Dipl at 1.8M.
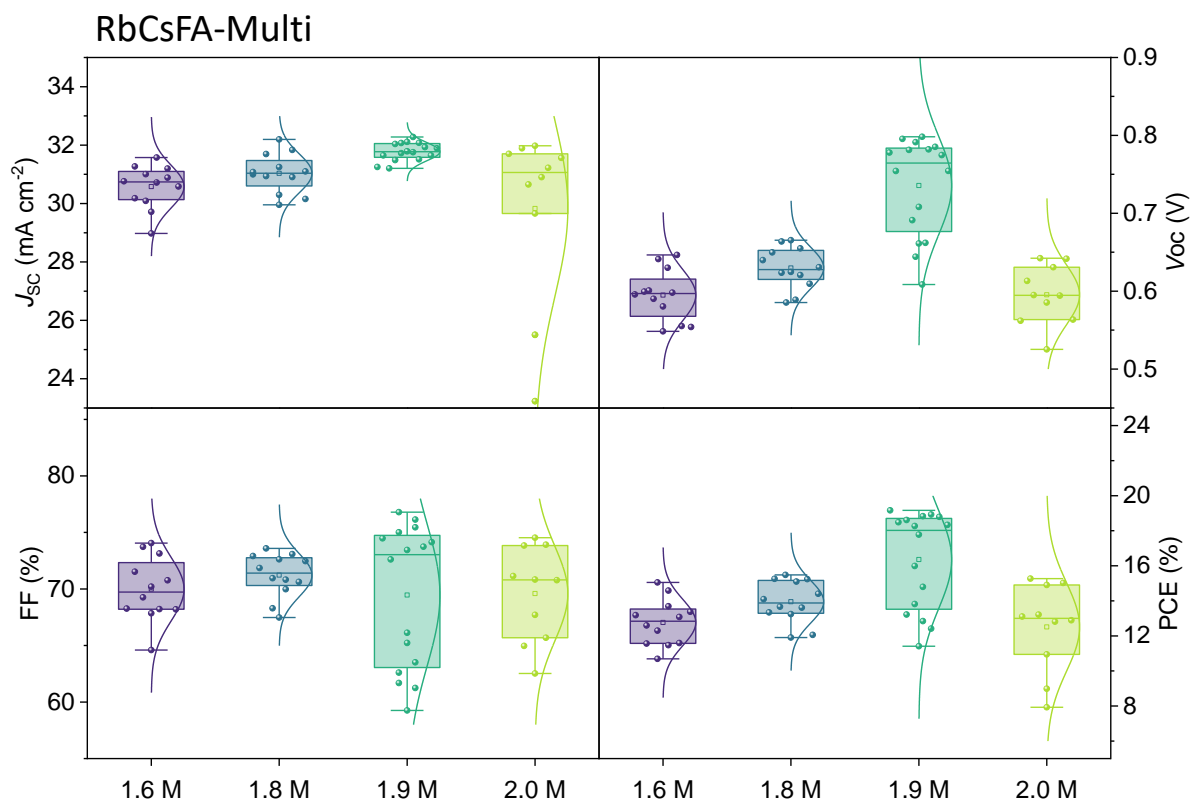
Figure S14. Box plot showing the distribution of the photovoltaic parameters for the solar cells fabricated with RbCsFA-Multi perovskite at different molarities of the total solution.
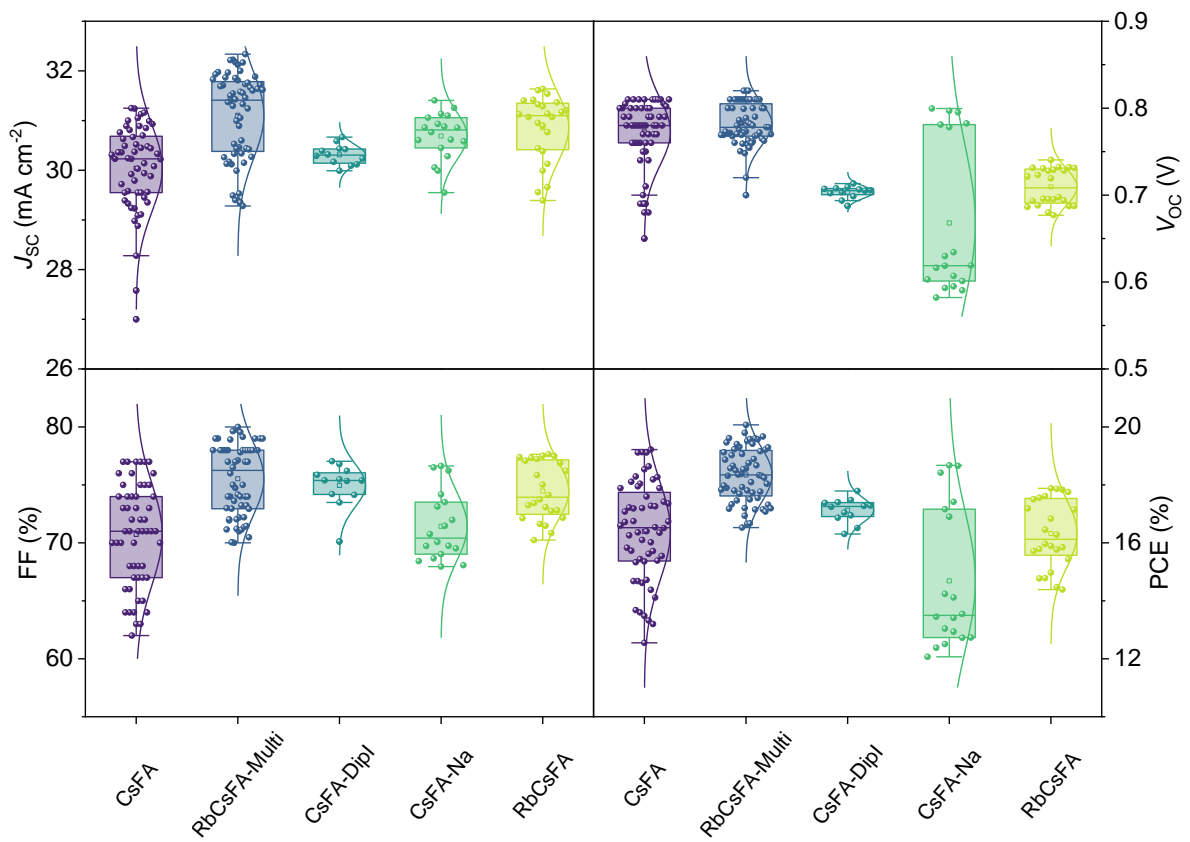
Figure S15. Box plot showing the distribution of the photovoltaic parameters for the solar cells fabricated with CsFA and RbCsFA-Multi. The statistics include over ~30 devices CsFA and RbCsFA-Multi and around 12-24 devices for CsFA-DipI, CsFA-Na and RbCsFA.
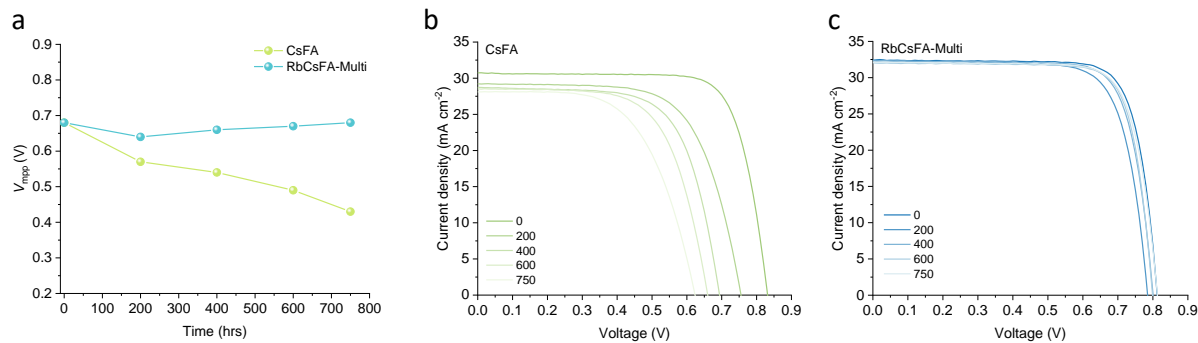
Figure S16. a) V_{MPP} evolution and b) *J-V* curves measured throughout the MPP experiment for CsFA and RbCsFA-Multi device. V_{MPP} are directly extracted from the *J-V*s. It's crucial to emphasize that we conducted stability measurements for the Maximum Power Point (MPP) without utilizing an MPP tracker. Instead, we maintained a fixed voltage during the experiment. Strictly speaking, our approach can be viewed as a quasi-MPP experiment. Nevertheless, it is noteworthy that the Voltage at the Maximum Power Point (V_{MPP}) exhibited remarkable stability throughout the entire experiment. This unequivocally indicates that our measurement conditions closely approximate the actual MPP, justifying our use of this terminology.

Table S3. Photovoltaic parameters of the CsFA cell used for MPP stability and V_{MPP} at different intervals extracted from the above *J-V* curves.

Time (h)	J_{SC} (mA/cm²)	V_{OC} (V)	FF (%)	PCE (%)	V_{MPP} (V)
0	30.74	0.83	76	19.50	0.68
200	29.24	0.76	66	14.68	0.57
400	28.73	0.69	67	13.42	0.54
600	28.52	0.66	65	12.31	0.49
750	28.11	0.62	60	10.54	0.43

Table S4. Photovoltaic parameters of the RbCsFA-Multi cell used for MPP stability and V_{MPP} at different intervals extracted from the above *J-V* curves.

Time (h)	J_{SC} (mA/cm²)	V_{OC} (V)	FF (%)	PCE (%)	V_{MPP} (V)
0	32.40	0.81	78	20.64	0.68
200	32.38	0.78	75	19.09	0.64
400	32.33	0.80	77	20.03	0.66
600	32.34	0.79	77	20.06	0.67
750	32.14	0.81	77	20.21	0.68
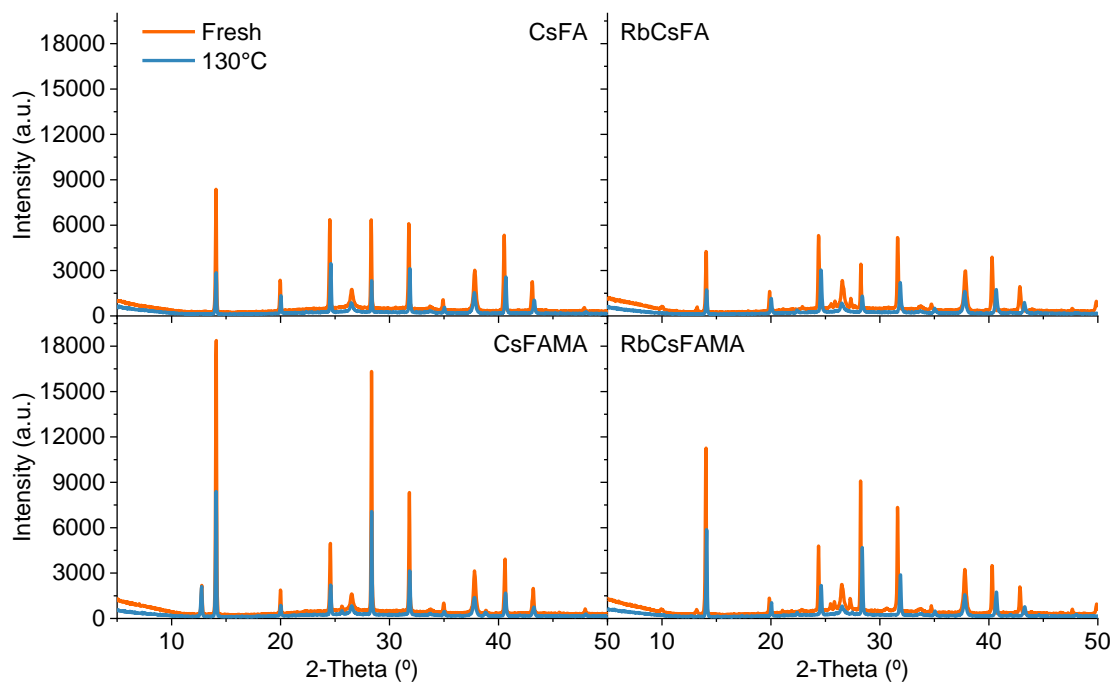
Figure S17. XRD pattern of CsFA, RbCsFA, CsMAFA, and RbCsMAFA perovskites films before (orange) and after (blue) annealing at 130°C for 3 h.
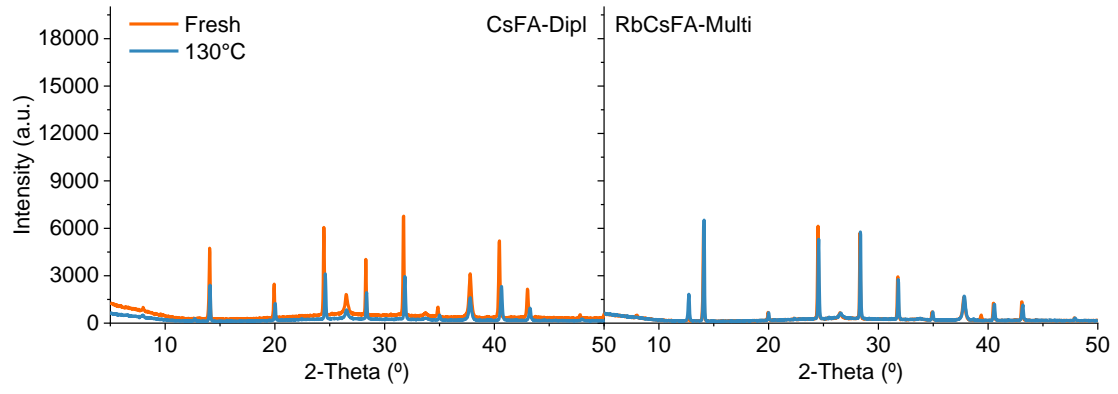
Figure S18. XRD pattern of CsFA-Dipl and RbCsFA-Multi perovskite films before (orange) and after (blue) annealing at 130°C for 3 h.
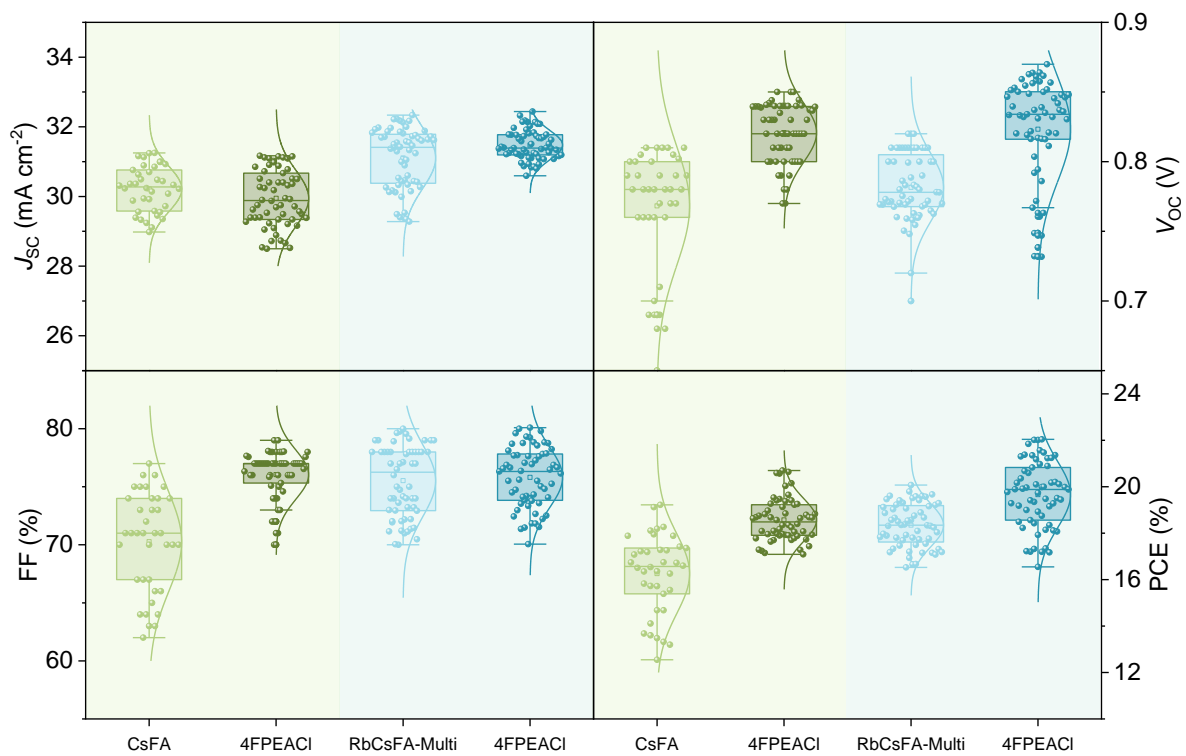
Figure S19. Box plot showing the distribution of the photovoltaic parameters for the solar cells fabricated with CsFA and RbCsFA-Multi compositions with 4FPEACl interlayer modification between perovskite and C_{60} layers. The statistics include over ~30 devices for each type.
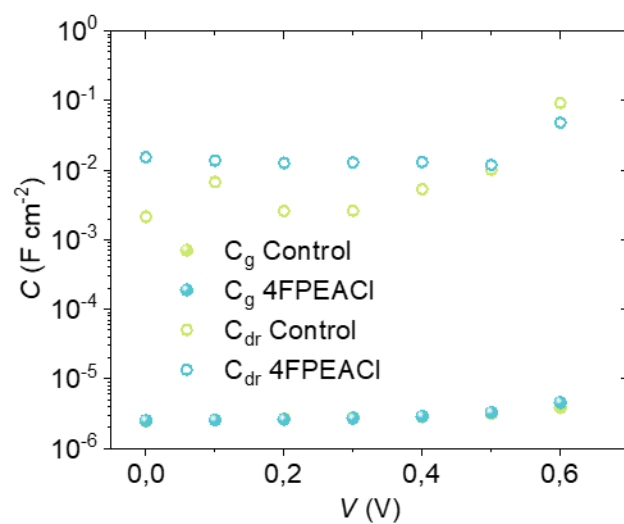
Figure S20. The geometric capacitance C_g and marginally higher C_{dr} extracted from impedance spectroscopy.